Differential Scrubbing in a Microchannel-plate Intensified CCD Detector

W. T. Thompson

Emergent Information Technologies, Inc., Space Science Division
NASA Goddard Space Flight Center, Code 682, Greenbelt, MD 20771, USA

ABSTRACT

One of the detector systems used for the Coronal Diagnostic Spectrometer instrument aboard the Solar and Heliospheric Observatory satellite is an intensified CCD camera. The intensifier section consists of a bare microchannel-plate detector proximity focused onto a phosphor, the light from which is then focused by a lens onto the CCD. Since the positions of the spectral lines is fixed on the detector, this leads to decreased efficiency in those areas of the detector where the strongest lines fall. The steps used to track this differential scrubbing of the detector in flight, and to remove these effects from the data, are described. Implications for future space missions are discussed.

Keywords: microchannel plate, extreme ultraviolet, detectors, space instrumentation, SOHO, CDS

1. INTRODUCTION

The Coronal Diagnostic Spectrometer (CDS) is an instrument aboard the Solar and Heliospheric Observatory (SOHO) satellite. CDS is a spectrographic instrument designed to measure emission lines from the solar corona and transition region in the extreme ultraviolet (EUV) range. Different sections of a Wolter II grazing incident telescope feed two spectrographs through a common selectable entrance slit. The Grazing Incidence Spectrograph (GIS) consists of a spherical grating illuminated at grazing incidence, feeding four microchannel-plate anode detectors strung out along the Rowland circle. The Normal Incidence Spectrometer (NIS) consists of two side-by-side stigmatic toroidal gratings illuminating a single intensified CCD detector, which for historical reasons is known as the Viewfinder Detector Subsystem (VDS). It is the in-flight performance of the VDS detector that will be considered here. A complete description of the CDS instrument is given by Harrison *et al.*[1]

The VDS detector is shown schematically in Figure 1, and is described more completely in Thompson *et al.*[2] EUV light from the two NIS gratings is focused onto the front face of the bare microchannel plate (MCP), which serves both as a photon detector and signal amplifier. A single Philips model G12-33 MCP wafer is used, with 12 μm pores on 15 μm centers, and L/D=40. The EUV photons are converted into electrons via the photoelectric effect on the front face of the MCP,[3] which are then amplified into larger clouds as they are accelerated down the MCP pores. A moderate voltage of 756 V is applied across the single MCP, so that the amplification is in the linear regime, well below saturation. The electron cloud exiting from the back of the MCP is proximity focused onto a P-20 phosphor coated on a fiber optic output window. The visible radiation light thus produced is focused via a lens onto a SITe (formerly Tektronix) 1024×1024

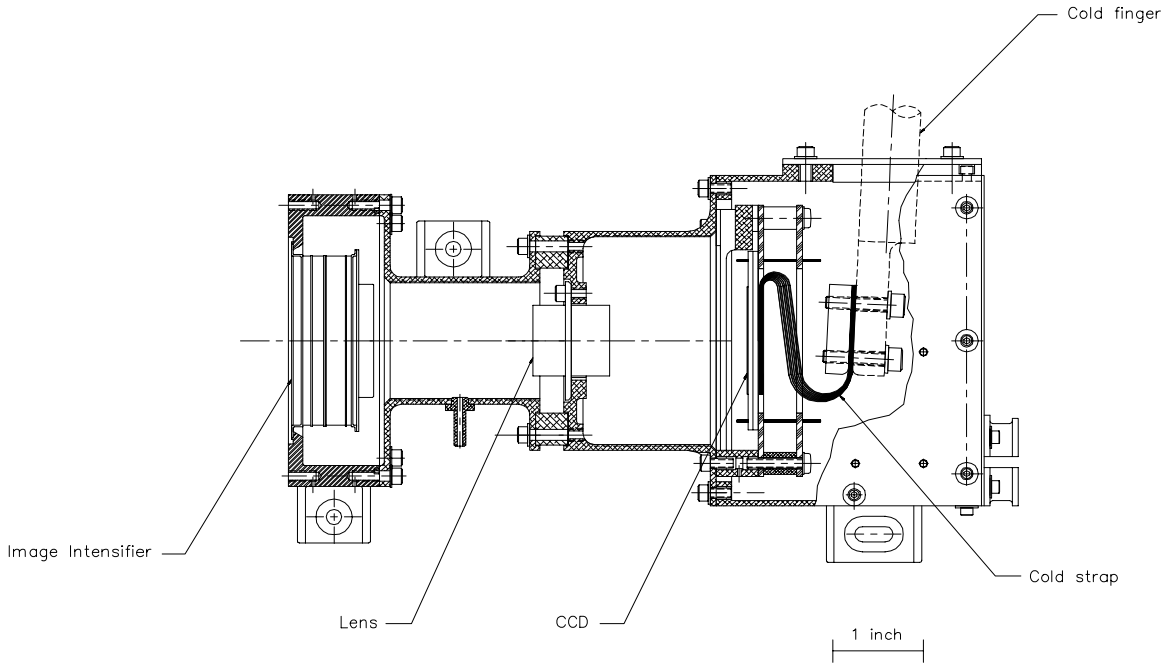

Figure 1. Schematic of the VDS detector, showing the MCP intensifier, the lens assembly, the CCD, and the cold strap and finger.

CCD with 21 μm square pixels. The signal is derived by measuring the total charge in a CCD well during the integration period—this allows for much higher count rates than is possible in a photon counting detector.

The NIS spectrograph consists of two side-by-side stigmatic toroidal gratings placed on the Rowland circle. Each of these gratings is tilted slightly, so that the two spectra illuminate different portions of the detector. The illumination pattern thus produced is illustrated in Figure 2, which shows some sample data taken in flight. The upper spectrum, known by the acronym NIS-1, ranges from 31–38 nm, while the lower spectrum (NIS-2) ranges from 51–63 nm. The arrow marks a known defect in the MCP, which falls within the NIS-1 spectral range, but in an area where it does not affect any spectral lines. Some cosmic ray events within the CCD are also visible—these vary from exposure to exposure. Most of the cosmic ray events in this 5-image composite have already been filtered out in the software processing. The image is displayed logarithmically to bring out the full dynamic range. In normal CDS observations, only the parts of the CCD containing the spectra are read out and telemetered to the ground. Most CDS observations only send small windows around selected spectral lines to conserve telemetry usage.

It is a well-known effect that MCPs exposed to radiation will gradually lose efficiency.[4,5] This process is known as scrubbing, and is caused by changes in the structure of the channel wall surfaces induced by the accumulated flux of electrons over time. Since the positions of the spectral lines on the detector do not change, the greatest amount of scrubbing will occur at the locations of the brightest spectral lines. We say that the lines burn into the detector. Another source of burn-in is exhaustion of the phosphor behind the MCP. The procedures used to monitor in flight the combined burn-in from these two mechanisms, and to correct the burn-in effects in the data, are discussed below.

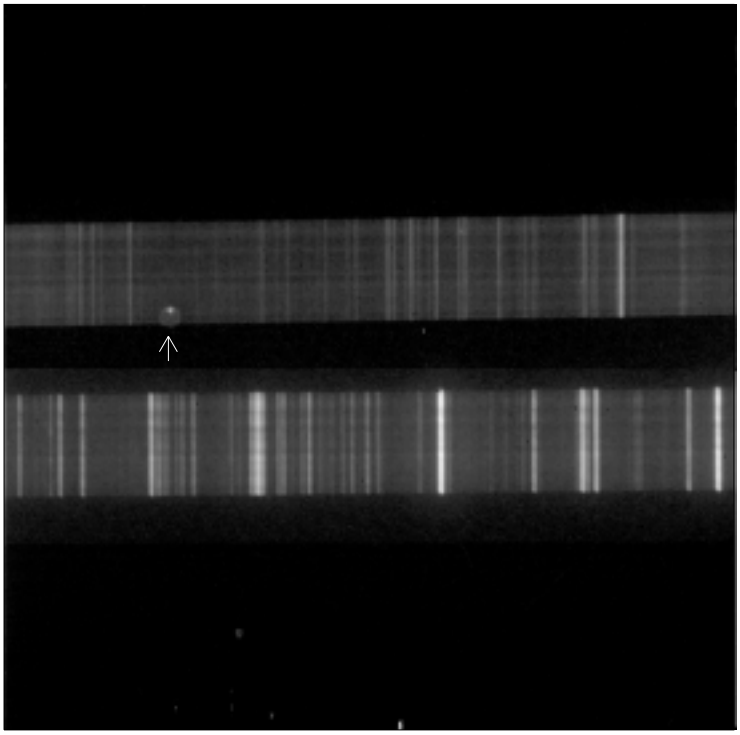

Figure 2. The illumination pattern of the NIS spectrograph on the VDS detector. The upper spectrum (NIS-1) ranges from 31–38 nm, while the lower spectrum (NIS-2) ranges from 51–63 nm. The image is displayed logarithmically to bring out the full dynamic range. The arrow marks a known defect in the MCP.

SOHO was launched on 2 December 1995. A "cruise phase" of several months was required for the spacecraft to reach its nominal orbit around the inner Lagrange point between the Earth and the Sun, although instrument operations generally began well before the end of this cruise phase. CDS/NIS observations of the Sun began on 5 February 1996. Because of SOHO's special position in space, the Sun is always visible, and observations are made 24 hours per day. After instrument commissioning, operations proceeded without interruption until 25 June 1998 when an accident caused SOHO to offpoint from the Sun and lose power for several months. Sun pointing was restored on 16 September 1998, and normal NIS solar observations were resumed on 2 October 1998. During the interim when SOHO was pointed away from the Sun, the instruments experienced extreme temperature conditions. The temperature of the CDS spectrometer section was measured to be close to 80° C when contact was re-established with the spacecraft, and it is believed that the instrument was even hotter for an extended period of time during the out-of-contact period. Although the instrument was recovered, it experienced a number of changes which can be attributed to the extreme heat. Some of these changes have an impact on the burn-in calibration. Therefore, in this report, we will only examine the effect of the differential scrubbing from the beginning of the mission until the loss of contact in June 1998. Some of the implications on the scrubbing correction of the instrument changes caused by the accident will be discussed at the end of the report.

2. THE OBSERVATIONS

There are three aperture slits which are most commonly used with the NIS. Two of these, slits #4 and #5, are narrow slits of dimensions $2'' \times 240''$ and $4'' \times 240''$ respectively (in the plate-scale of the telescope, 25 μm/arcsec), suitable for resolving spectral lines. Because of the resolution of the NIS spectrometer, the primary differences between these two slits on the detector are spatial resolution and intensity—the observed line widths are very close to being the same. Approximately 95% of the NIS observations are made with one or the other of these narrow slits. The remaining 5% of the time, except for a few isolated cases, is spent observing with a wide $90'' \times 240''$ aperture (slit #6) suitable for obtaining spectroheliogram images in the stronger lines. Sometimes this wide slit is known as the "movie" slit, because of its use in making high cadence time series observations.

One of the benefits of the movie slit is that it allows the burn-in due to the more commonly used narrow slits to be directly observed and measured. Figure 3 shows this quite clearly. In this figure, a movie-slit observation made early in the mission is compared with one made about two years later. In the later data, dark lines are clearly visible down the center of the spectroheliogram formed by each strong spectral line. These dark burned-in lines occur where the narrow-slit spectral lines fall on the detector.

Two special studies are used to monitor these narrow slit burn-ins. Both make use of the $90''$ wide movie slit. The first simply observes a variety of quiet Sun targets, depending on the combination of a number of such images to wash out solar features. The second study utilizes a special operation mode to move the instrument pointing during the exposures, so that the solar features are smoothed out by the motion. Both of these studies are discussed below. In addition, the regular synoptic observations of CDS are used to help monitor the behavior of the instrument.

3. CALIBRATING THE NARROW SLIT BURN-IN

In order to track the burn-in of the detector over time, a special study is run several times a week. This study, known in the CDS planning software by the acronym NIMCP, takes three exposures with the $90''$ movie slit at slightly different spatial positions, followed by a single exposure with the $2''$ narrow slit. The first step in the processing of these data is to remove all known detector effects, except the burn-in correction. The three movie-slit measurements are then averaged together to help wash out solar features. To further wash out the effect of solar spatial variation, a number of NIMCP observations are averaged together, usually over about a two-week period. Finally, to help wash out any solar features which remain, the data are averaged in the vertical direction. The burn-in measured by this technique will then be an average value over the length of the slit. The same averaging procedure is also applied to the data taken with the narrow slit, for comparison, except that here a correction is made for estimated burn-in effects.

The analysis of the resulting average profiles is a multistep process. First, a region of the spectrum is selected. The narrow slit spectrum from this region is then fitted to extract the intensities in each line. These intensities are then used to develop a model of what the same spectrum would look like if observed with the movie slit. The model is then adjusted to fit to the observed average movie-slit profile, with the narrow slit burn-ins modeled with Gaussian functions. Figure 4 shows a sample of the data used to perform this analysis. The lower dashed line shows the narrow slit profile from the dataset being analyzed, while the lower solid line is the fitted spectrum.

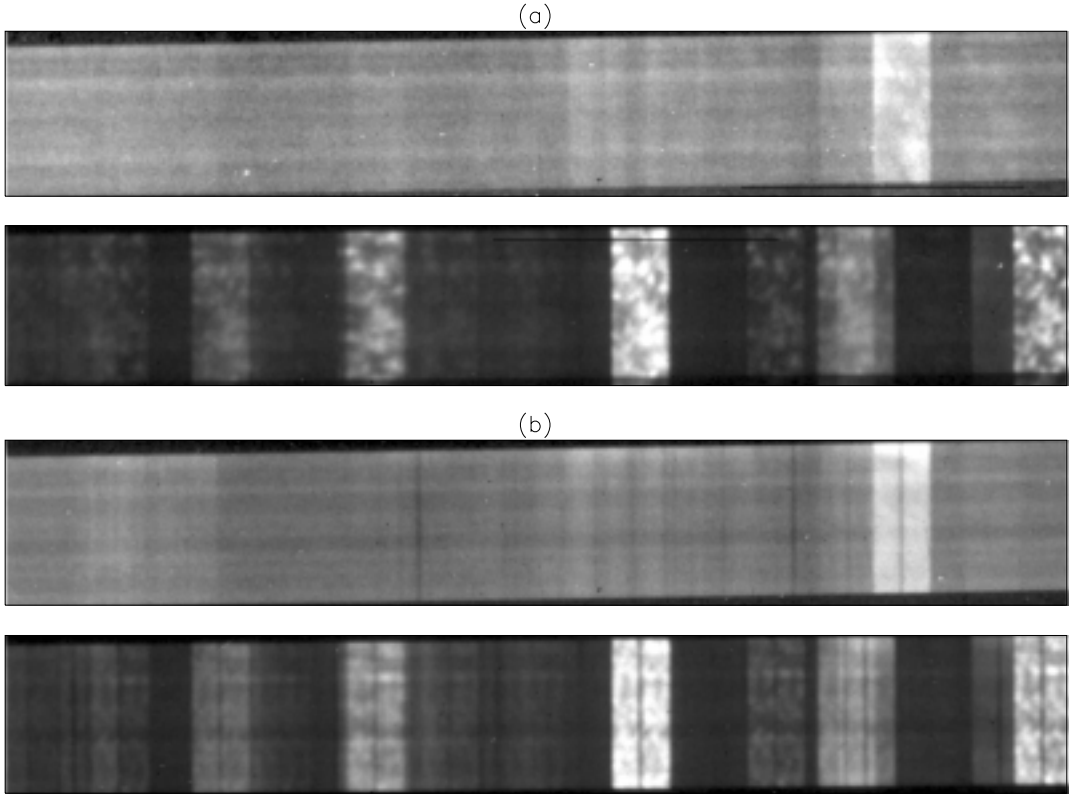

Figure 3. a) An observation from early in the mission, on 15 March 1996, before any significant burn-in occurred. The CDS 90″ wide "movie" slit (#6) is used, showing spectroheliogram images wherever there is a strong emission line. b) An observation from approximately two years later, on 30 April 1998, clearly showing the burn-in of strong lines. These burn-ins occur down the center of each strong spectroheliogram image, where the narrow slit spectral lines would illuminate the detector.

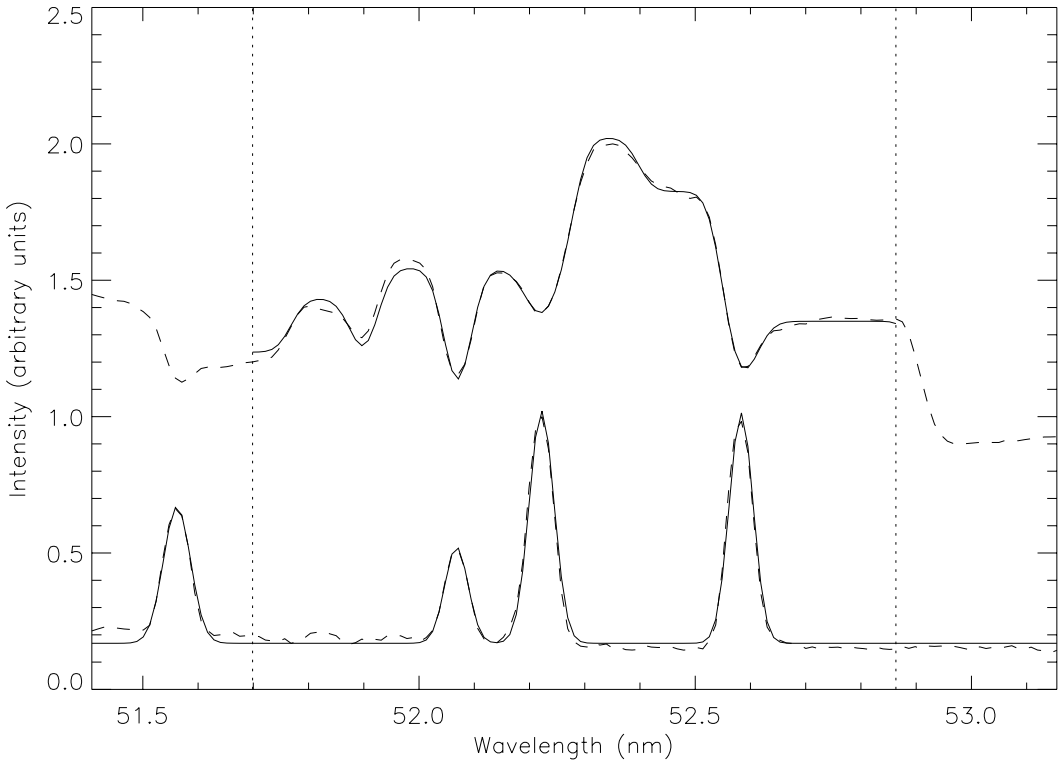

Figure 4. Sample data showing the burn-in fitting process. The data is on an arbitrary scale. See the text for an explanation of the different line styles.

The upper dashed line is the observed movie slit profile, and again the solid line is the fit to this profile. The vertical dotted lines mark the limits of the range considered in the fit to the movie slit data. Burn-in profiles are measured for the three emission lines between the vertical dotted lines. The left-most emission line is used only to refine the shape of the fit to the movie slit data. Note that an apparent burn-in profile at 51.9 nm also appears in the fitted data, even though no emission line appears there. This feature is actually an artifact of the overlapping movie-slit profiles.

Fitted burn-in parameters from a series of such analyses over the lifetime of the mission leads to plots like those shown by the "*" symbols in Figure 5. This plot shows the burn-in due to the exposure of the detector to the very strong He I line at 58.4 nm, which is the strongest line observed by the VDS, and consequently shows the greatest amount of burn-in. It was found that most of the lines could be well fitted with a curve of the form

$$\beta = a_0 + a_1 \exp(-\Delta t / a_2) \tag{1}$$

with the constraint that $\beta \leq 0$. Expressing the data by an empirically-derived analytical curve allows the data to be interpolated or extrapolated to any date. For some of the stronger lines, such as the 58.4 nm line shown in Figure 5, two exponential curves were summed together (each with $\beta \leq 0$) to adequately replicate the behavior of the data points. The RMS differences between the measured data points and the fitted curve are typically on the order of 3% or less, and appear to be randomly distributed.

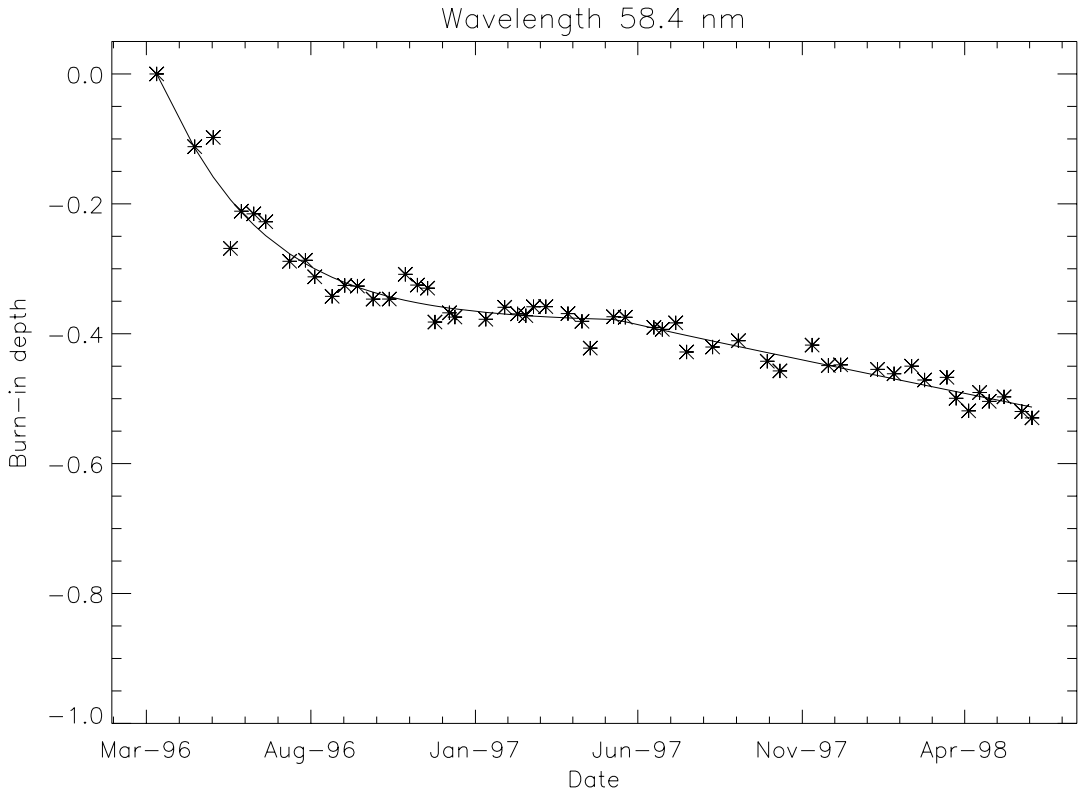

Figure 5. Burn-in measurements of the He I line at 58.4 nm, where 0 represents no burn-in, and -1 represents complete burn-in. The "*" symbols show the measured burn-in values, and the curve shows an empirical curve fitted to the data. This line is the strongest line observed by the VDS, and shows the greatest amount of burn-in.

Table 1 shows the list of all lines with known burn-ins of their narrow slit profile, together with their central burn-in depths as of 24 June 1998. The CDS calibration routines automatically correct the data for these burn-in profiles. Figure 6 shows the effect of this correction on the same data shown in Figure 3b.

The amount of burn-in of most lines can be correlated to their intensity in an average quiet Sun profile. For example, the line with the strongest amount of burn-in, at 58.4 nm, is also the line which is typically the strongest in any observation. The same goes for the O V line at 63.0 nm. However, there are a few lines which show significant amounts of burn-in even though these lines are not particularly strong in the quiet Sun, or may not even be present at all in some observations. This is particularly true of the Fe XVI lines at 33.54 nm and 36.08 nm. The significant amounts of burn-in which are seen at these line locations can only be attributed to exposure to active regions, where those lines become very strong. The 33.54 nm line is a particularly good example of this. In the quiet Sun, this line is blended with a cooler Mg VIII line at 33.52 nm, which indeed usually dominates in the quiet Sun. However, the location of the burn-in is clearly centered on the Fe XVI line, showing that it is active region observations which is producing the burn-in.

Wavelength (nm)	Burn-in	Wavelength (nm)	Burn-in
31.50	-0.070	52.08	-0.273
31.62	-0.058	52.23	-0.098
33.42	-0.077	52.59	-0.147
33.54	-0.257	53.71	-0.243
34.11	-0.033	53.83	-0.081
34.20	-0.037	55.35	-0.102
34.51	-0.062	55.45	-0.313
34.74	-0.082	55.54	-0.090
34.99	-0.072	56.29	-0.115
35.21	-0.076	56.84	-0.106
35.27	-0.073	57.41	-0.072
35.60	-0.098	58.44	-0.520
36.08	-0.222	59.96	-0.182
36.45	-0.128	60.76	-0.268
36.78	-0.075	60.84	-0.032
36.81	-0.309	60.98	-0.374
		62.50	-0.289
		62.98	-0.463

Table 1. Lines with known narrow-slit burn-ins as of 24 June 1998.

4. THE FLAT FIELD CALIBRATION

Another observation which is used to measure the amount of burn-in on the detector is FFCAL. Like NIMCP, this program observes with the 90″ wide movie slit. However, instead of telemetering down the entire NIS spectral ranges, seven data windows in the brightest areas of the spectra are selected for telemetry. This allows more rapid turnaround between exposures, and many more exposures are taken in the same amount of time. During the run of the study, the CDS pointing mechanisms are slewn back and forth. This will cause some of the exposures to be taken while the instrument is in motion, resulting in a smeared image on the detector. By averaging together only those exposures which show a smeared Sun, an essentially flat exposure image is built up in each data window, as demonstrated in Figure 7.

The FFCAL observations are less frequent than the NIMCP observations, and don't cover all the lines with burn-in. However, the signal-to-noise in these images are much higher, and are less sensitive to solar features. They help refine the results of the NIMCP measurements, and also serve as a useful testbed for the burn-in correction algorithms. In particular, the FFCAL measurements are useful for determining the behavior of the shape of the burn-in profile with time.

5. BURN-IN LINE PROFILES

As spectral lines get burned into the detector, the cores of the lines will burn in faster than the line wings. This will cause uncorrected line profiles to not only decrease in strength, but also slowly

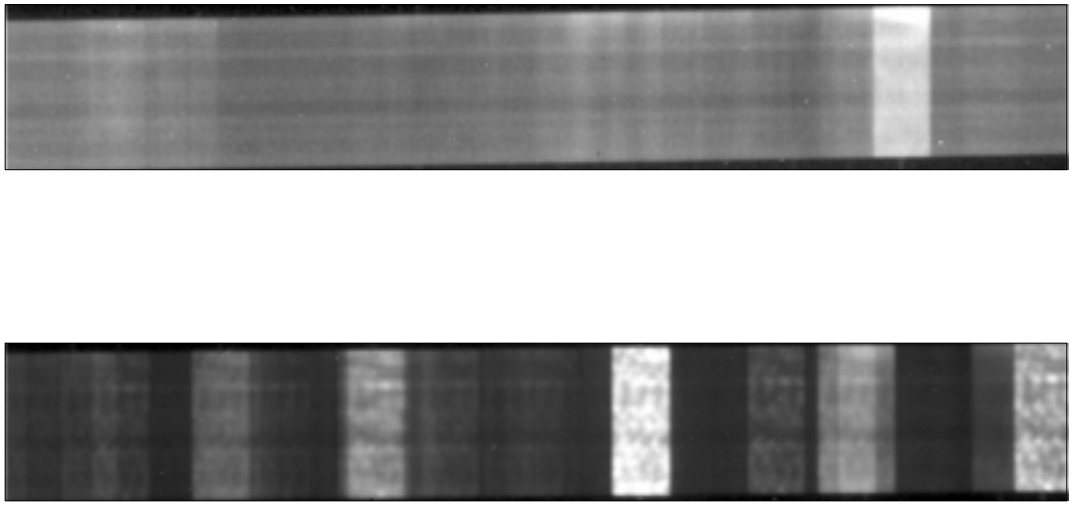

Figure 6. The data of Figure 3b after the narrow-slit burn-in correction has been applied.

increase in apparent width. By modeling the burn-in with a Gaussian profile, this differential affect across the line should be accounted for, and the original line profile should be restored.

Detailed analysis of the burn-in line profiles show that in the lines with the greatest amount of burn-in, the profiles start to deviate from a Gaussian. This is caused by the fact that the burn-in of the line cores will start to slow down after reaching a depth of ~30% (*c.f.* Figure 5), while the wings of the line are still going down. In part, this effect is modeled by allowing the burn-in widths to increase with time. However, this does not entirely replicate the behavior of the burn-in profiles.

In a strongly burned in line like 58.4 nm, a correction algorithm based on Gaussian profiles will restore the original solar intensity in the core of the line, but undercorrect in the line wings. The discrepancy between the estimated intensity in the line cores, and the solar intensity is on the order of 2%. This has the effect of artificially narrowing the line profile.

In order to improve the burn-in line profiles, the Gaussian function must be modified to include a flattening parameter. Analysis of FFCAL observation shows that a function of the form

$$\begin{aligned} \sigma' &= \frac{2\sigma}{1+\sqrt{1+2|f|/\ln 2}} \\ z &= (x-x_0)/\sigma' \\ w &= z^2/(|f|+|z|) \\ y &= \beta e^{-w^2/2} \end{aligned} \tag{2}$$

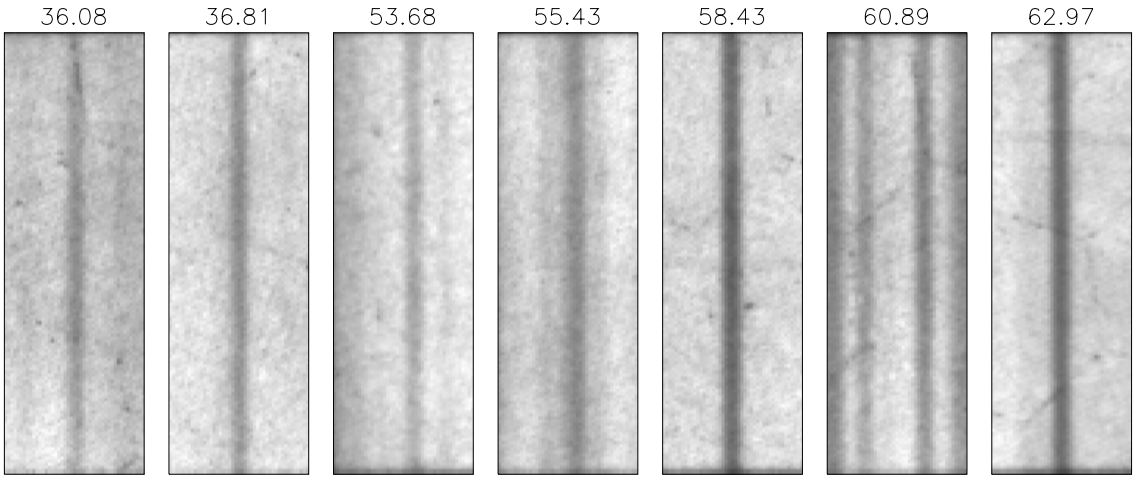

Figure 7. The response of the VDS detector to an essentially flat radiation field, in seven selected data windows. The effect of a flat radiation field was simulated by averaging together a number of exposures where solar features were smeared out by moving the instrument during the exposure. As well as the narrow-slit burn-in patterns of strong lines, one can also see the hexagonal pattern of the fiber-optic output window of the image intensifier.

appears to well describe the behavior of the more strongly burned in lines. The parameters β, x_0, and σ are the normal Gaussian parameters describing the depth, position, and width. The additional parameter, f, describes the amount of flattening. When f is zero, then $\sigma' = \sigma$, $w^2 = z^2$, and one obtains the normal Gaussian formula. The transformation from σ to σ' is done so that the width parameter σ is directly comparable to that of a normal Gaussian. The full-width-half-maximum of a profile given by equation 2 will be independent of the parameter f. More work is needed to show how f varies with time. For the present, it is assumed that f is constant with time, which is consistent with the data that we presently have.

There appears to be some evidence that the center location of the burn-in profiles has shifted with time. This is most easily seen with the FFCAL observations, where the center positions of burn-in patterns due to the 58.4 nm and 63.0 nm lines both appear to have shifted by 0.3 pixels between September 1996 and May 1998. However, because there were no runs of FFCAL between September 1996 and September 1997, it's difficult to tell exactly how the position changes with time. For example, is this shift best modeled by a linear function, or as an event? There's also some indication of a shift in the NIMCP measurements, toward the long wavelength end of the NIS 2 spectrum. At the present, we model the shift with a linear fit.

Even with the best modeling of the burn-in shapes based on movie slit data, there's still a strong signature of the burn-in in the measured spectral line widths with time. This effect is greatest in the 58.4 nm line, where the average width has decreased by $\sim$8% since the beginning of the mission. Evidently, the shapes as measured by using the movie slit do not entirely represent the situation when one of the narrower slits is used. One possible explanation lies in the resolution of the detector itself. There's a small loss of resolution between the output of the MCP wafer and the phosphor, and also in the transfer lens between the fiber-optic output window and the CCD. This may distort the appearance of the burn-in profile seen when the movie slit is used, particularly in the wings.

6. SPATIAL VARIATION ALONG THE SLIT

All the analysis of narrow-slit burn-in effects so far considered has assumed that the time-averaged behavior will be such that each part of the slit will receive a uniform dosage. Detailed examination of the data shows that this assumption holds for most of the lines. The exceptions are those lines whose burn-in values can be attributed to active regions, e.g. Fe XVI 33.54 nm and 36.08 nm. In those lines, there is a slight increase in the amount of burn-in in the center of the slit, suggesting that active regions tend to be selectively centered on the detector.

7. THE EFFECT OF THE MOVIE SLIT

CDS is an instrument that runs a wide variety of observing programs on ever-changing solar targets. However, there is a synoptic set of observations which is run on a daily basis. The CDS synoptic program consists of nine NIS rasters covering the solar meridian from the north pole to the south pole, in four lines: He I 58.4 nm, O V 63.0 nm, Mg IX 36.8 nm, and Fe XVI 36.1 nm. The combination of regular daily coverage, plus the large amount of solar area observed, offers the opportunity to monitor the long term variation in the CDS detector gain.

Gaussian profiles were fitted to the average line profiles for the central synoptic image each day. (An earlier version of the synoptic program, with only eight rasters, was used for the first few

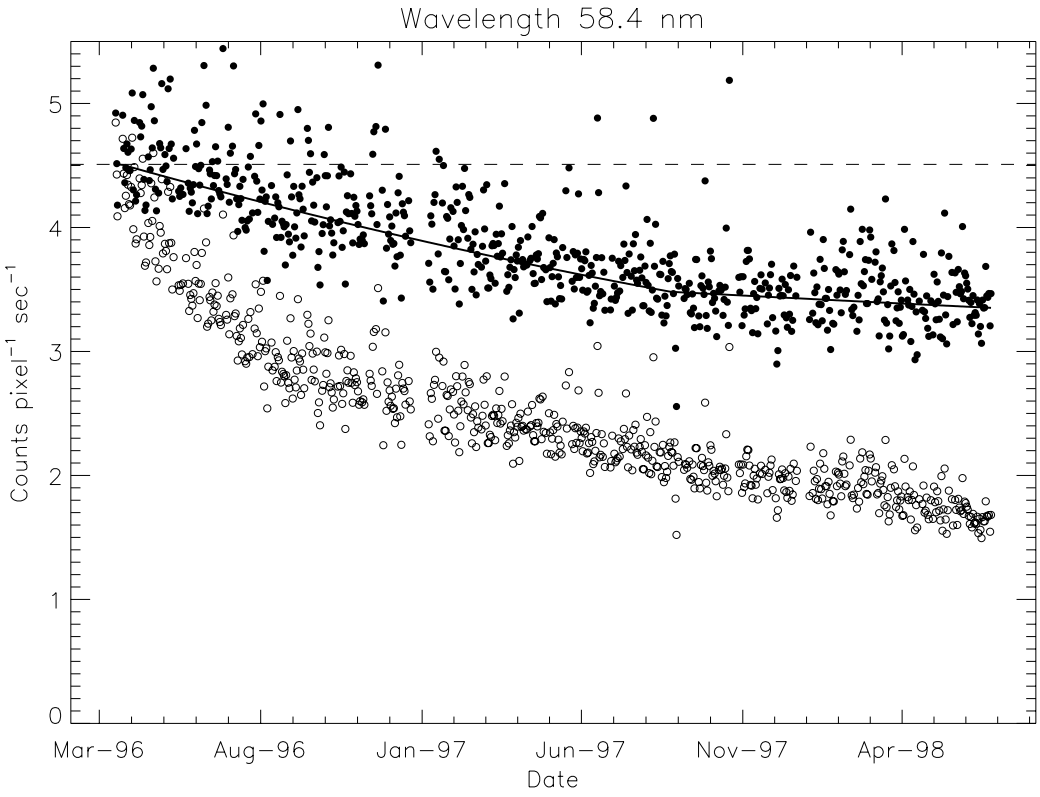

Figure 8. The peak intensity values of the He I 58.4 nm line, derived from the daily synoptic images. The open circles are the data without the narrow-slit burn-in correction applied, and the filled circles are with the correction applied. The solid line represents a fitted curve, and the dashed line represents the assumed 58.4 nm intensity, as explained in the text.

weeks of the mission, and was also included in the analysis.) Since the line width is known to vary with time, due to instrumental effects, only the peak of the intensity profile was examined, rather than the integrated intensity. Figure 8 shows the daily values of the peak intensity of the 58.4 nm line. The open circles are for data without the narrow slit burn-in correction, and the filled circles are for the same data with the correction applied. Although the correction does make a significant difference in the derived intensities, there is still a slow drift down, even after the correction has been applied. Another instrument on SOHO, the Solar EUV Monitor, measures the absolute irradiance of the Sun in a band dominated by the related He II 30.4 nm line. These data show no such variation over this period, which suggests that the variation seen in Figure 8 is not solar in nature. The O V 63.0 nm line, which is the second strongest line seen by VDS, shows similar behavior, although less strongly. No such long-term effect is seen in Mg IX 36.8 nm, although because of the high formation temperature of this line, it is more sensitive to solar variability which confuses the analysis. (The Fe XVI line is associated with strong solar activity, and thus is not conducive to this kind of analysis.)

It appears from Figure 8 that there is an additional component to the loss of gain in the VDS detector, besides the narrow-slit burn-in. One possibility is that there is an additional burn-in component from the use of the 90″ wide movie slit. This is supported by the fact that the residual

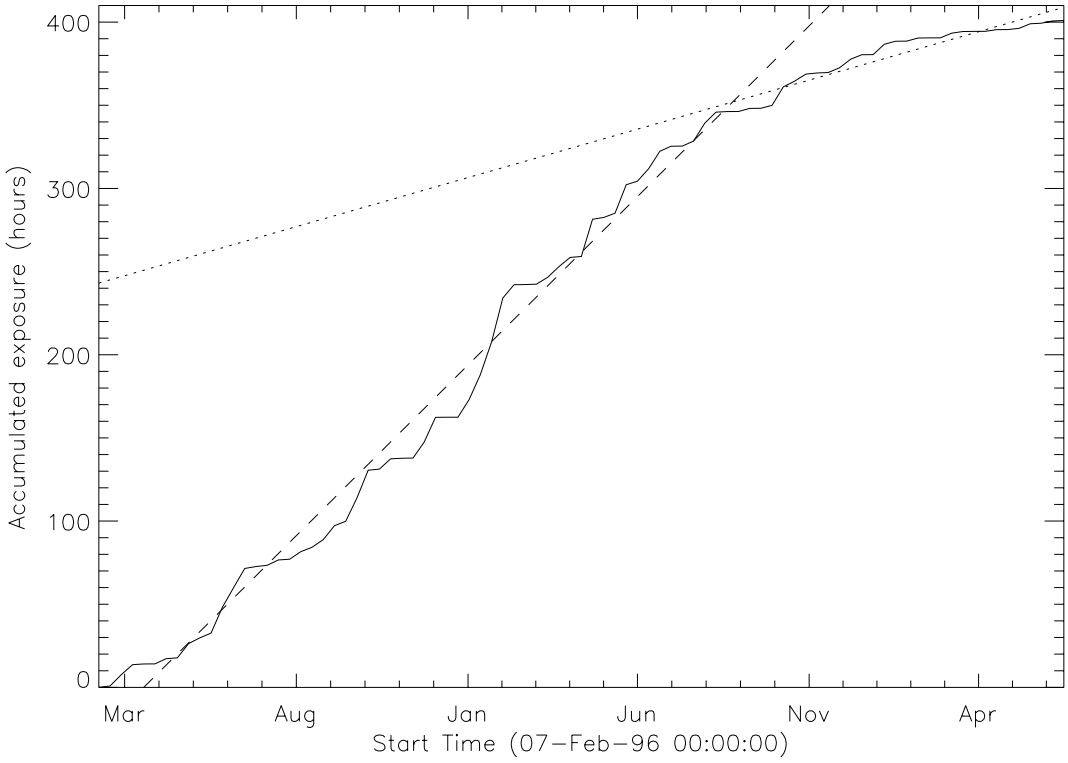

Figure 9. The accumulated exposure of the VDS detector to the 90″ wide movie slit. The dashed and dotted lines are linear fits to the earlier and later data respectively.

gain loss appears to be related to line strength. The dashed line in Figure 8 shows the interpolated 58.4 nm peak intensity at the beginning of the mission, when little or no burn-in had occured on the detector. The solid line is a polynomial fit to the data. The ratio of the two curves should give the amount of burn-in due to the movie slit.

Note that the movie-slit burn-in shown in Figure 8 appears to level off after about June 1997. This is not because the burn-in reached a plateau, but because the use of the movie slit decreased dramatically at about this time. This is demonstrated in Figure 9, which shows the accumulated exposure time of the VDS detector to the movie slit. Up until about August 1997, the total exposure time is increasing roughly linearly, as shown by the dashed line fit to the earlier data. After that time, however, the accumulated exposure is climbing much less rapidly, as shown by the dotted line fit. The effect of this can also be seen in the narrow slit burn-in data. Since the rate of burn-in slows down with increased exposure, the movie slit burn-in will affect pixels outside the line centers more than it will already well burned-in line center pixels. This will tend to decrease the apparent narrow-slit burn-in, by depressing the surrounding pixels. When the movie slit started to be used less, the narrow slit burn-in appeared to increase in the more burned-in lines. This can be seen as a change in slope in Figure 5. In actually, the line centers are not burning in more rapidly—no change in slope can be seen in the uncorrected data in Figure 8—it's just that the areas immediately outside the lines are burning in less rapidly.

The solid curve in Figure 8 has been calculated from an adjusted time based on the usage data

from Figure 9. Dates after the intersection of the two linear fits to the usage data were adjusted to the date represented by the earlier (dashed) fit, to simulate a constant usage rate with time. The horizontal dashed line in Figure 8 represents the interpolation of the solid line to 21 March 1996, which is the date that the dashed line in Figure 9 interpolates to zero usage.

Because most observations with the NIS only download selected data windows, there's no *a priori* way to build up an exposure history for each pixel. In order to extrapolate the behavior of the 58.4 nm line to other areas of the detectors, an average quiet Sun profile was built up from a number of movie-slit observations. These observations were selected from the earliest part of the mission, so that they themselves should not be affected by any loss of detector gain over time. The average derived profiles are shown in Figure 10, normalized to unity at 58.4 nm. (Some smoothing has been applied.) The extrapolation then makes the following assumptions:

- The spatial distribution of the cumulative exposure of the detector to solar radiation with the $90''$ movie slit is well represented by Figure 10, and that this exposure is evenly distributed vertically along the slit.
- The total exposure to the movie slit can be estimated from the two linear fits shown in Figure 9.
- The total movie slit burn-in at a given pixel as a function of time is related to the estimated total exposure through the ratio of the two curves shown in Figure 8.

Using these three assumptions, the total amount of movie slit burn-in as a function of time at any given point is estimated by the following method. The difference between the date of observation and 21 March 1996, adjusted if necessary for the change of slope after 24 August 1997, is multiplied by the average slit profile from Figure 10. This "effective time" represents the time at which the same amount of exposure would have been seen in the 58.4 nm line. The total amount of movie slit burn-in is then calculated by passing this "effective time" into the polynomial represented by the solid line in Figure 8.

The first of the above assumptions would be violated if a significant fraction of these observations were made of active regions. Active region observations with the movie slit would have two effects. First of all, higher temperature lines would increase in intensity out of proportion to the He I 58.4 nm line intensity, significantly changing the shape of the exposure profile from that shown in Figure 10. Second, the intensity pattern of an active region is much more highly structured than in the quiet Sun, which has the potential of yielding a non-uniform burn-in pattern. However, only occasional observations of active regions were made with the movie slit in the early part of the mission. When the potential for burning in the movie slit became clear, it was decided to not use the movie slit on active regions.

Figure 11 shows the uncorrected and corrected peak intensity of the O V line at 63.0 nm, which is the second brightest line in the NIS spectra. The extrapolated movie slit burn-in for this line, using the procedure outlined above, is superimposed as a solid line.

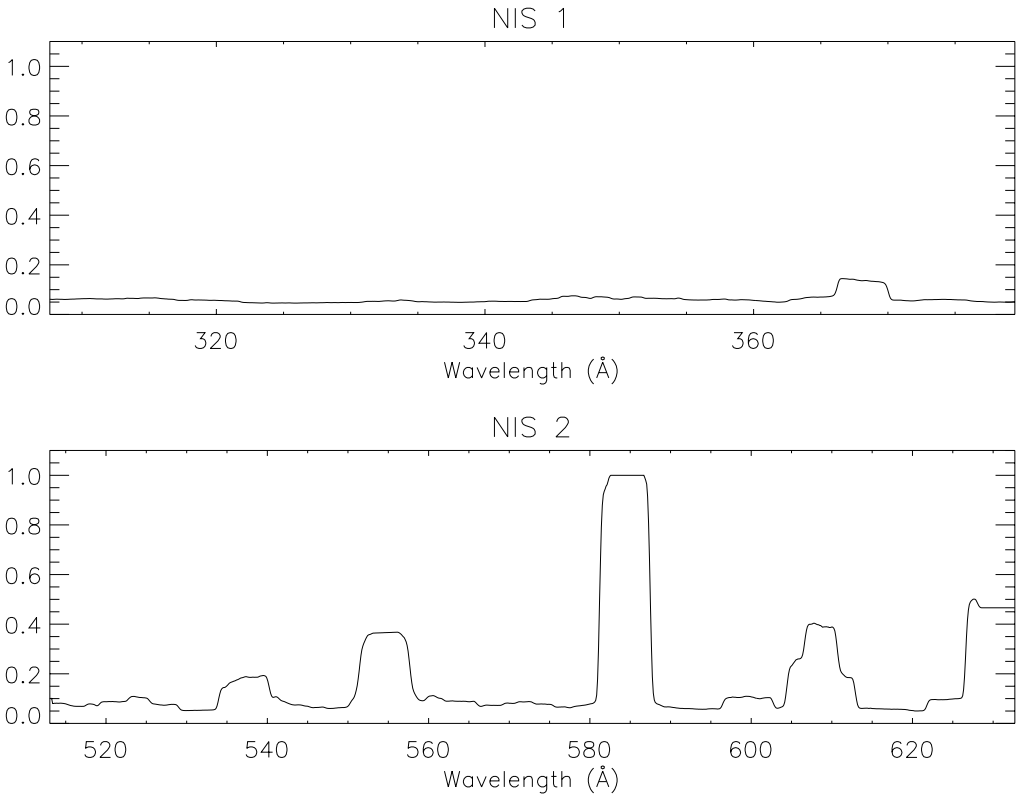

Figure 10. The average quiet Sun profile as observed with the 90″ wide movie slit. The data are normalized to unity at 58.4 nm.

8. CHANGES CAUSED BY SOHO'S ACCIDENT

As mentioned before, when SOHO lost attitude control and power in the summer of 1998, the CDS instrument was subjected to extremely high temperatures for a period of several months. When the SOHO satellite was recovered, it was found that the two NIS spectra had shifted positions on the detector, both horizontally and vertically. The spectral lines were shifted off of their narrow-slit burn-in patterns. Also, for the first time, the burn-in pattern from the movie slit could be seen. This is demonstrated in Figure 12, which shows a post-recovery FFCAL measurement from the movie slit image of the He I 58.4 nm line. The narrow slit burn-in profile from the accumulated pre-accident exposure is clearly visible on the left of the image. Careful examination also shows the start of the narrow slit burn-in at the new spectral line position down the center. The burn-in from pre-accident exposure to the movie slit is visible as a dark rectangle over most of the image. Pixels along the top of the image were never exposed to solar radiation before the accident, while pixels along the right side were only exposed to wavelengths much fainter than 58.4 nm. The amount of movie slit burn-in deduced from this image is compatible with the estimate derived from Figure 8 just before the accident, to within a few percent.

It also appears that the extreme heat experienced by CDS during the months when SOHO was without power actually reversed some of the burn-in effects on the detector. The narrow slit burn-ins measured after recovery are only about 80% of their values just before the accident. The overall

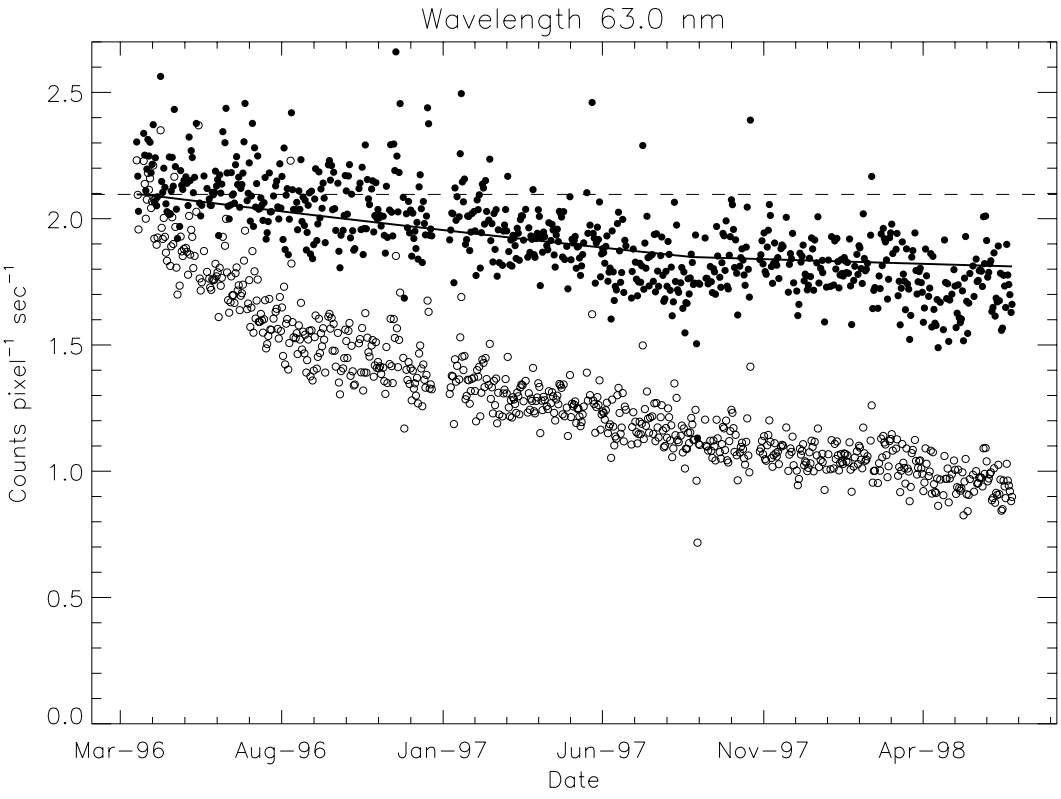

Figure 11. The peak intensity values of the O V 63.0 nm line, derived from the daily synoptic images. The open circles are the data without the narrow-slit burn-in correction applied, and the filled circles are with the correction applied. The solid line shows the assumed movie slit burn-in extrapolated from the He I 58.4 nm data from Figure 8 as modulated by the average movie slit profile from Figure 10. The dashed line represents the assumed intensity if there were no burn-in.

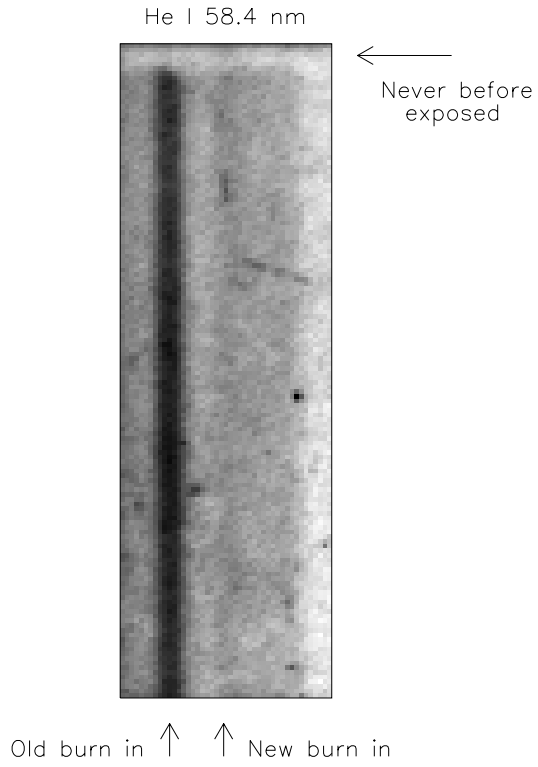

Figure 12. Post-recovery movie slit image produced by the He I 58.4 nm line. The pre-accident narrow slit burn-in is clearly visible on the left. The faint beginnings of the new narrow slit burn-in appear in a line running down the center of the image. Previously unexposed areas of the detector along the top and right side of the image are brighter than the area previously illuminated by the 90″ wide movie slit (dark rectangle).

detector sensitivity appears to be unchanged.

It's clear from Figure 12 that tracking the post-recovery burn-in pattern on the detector will be a more challenging task than before the accident. Each strong spectral line will have two narrow-slit burn-in profiles, one at the old location and one at the new. The new profile will deepen with time, while the old profile should gradually fade out as the pixels around it are exposed by the movie slit. There will also be two overlapping movie slit burn-in patterns, one old and one new, which will have to be independently monitored with time.

9. RELATIONSHIP OF BURN-IN TO CHARGE EXTRACTED

As discussed before, there's no direct way to determine the total amount of accumulated exposure at a given pixel location, since not all the data is telemetered down. However, one can estimate total amount of exposure with a few assumptions. Between first light in February 1996, and SOHO's accident in June 1998, the NIS instrument accumulated about 6421 hours of exposure with the $2'' \times 240''$ slit, 3204 hours with the $4'' \times 240''$ slit, and 401 hours with the $90'' \times 240''$ movie slit. If we assume that the average count rate in the core of the He I 58.4 nm line was 4, 8, and 20 counts/pix/s respectively, then the total exposure over the course of the mission was 1.8×10^8 detected photons from the two narrow slits alone, and 2.1×10^8 from all three slits combined. These numbers are based on average quiet Sun measurements, while the actual observations include active regions, coronal holes, and off-limb corona measurements. However, the increased exposure from active region observations should be at least partially offset by the decreased exposure from coronal hole and off-limb measurements. Therefore, the above estimates should be reasonably valid. To account for the higher flux from active regions, we will assume that the total exposure is between one and two times the above estimates.

According to preflight measurements, the electron gain in the MCP at 756 V is about 600 (594 ± 43) electrons for every detected photon. Therefore, the total exposure to all three slits represents an extracted charge of about $2.1–4.1 \times 10^{-8}$ C/pix. Each pixel is 21 μm square, so this is equivalent to 4.7–9.3 mC/cm^2. The corresponding loss in detector gain was approximately 63%, as shown by the open circles in Figure 8. The areas just outside the 58.4 nm narrow-slit line profile were exposed to about 0.63–1.26 mC/cm^2 by the much wider movie slit, and lost approximately 26% of detector gain, as shown by the closed circles in Figure 8.

10. CONCLUSIONS

Most of the burn-in of bright spectral lines on the VDS detector can be tracked and removed, based on the analysis of movie-slit observations such as NIMCP and FFCAL. The accuracy of this process appears to be on the order of 3% or less. However, once this is done, the following artifacts still remain in the data:

- There is an additional suppression of bright lines which cannot be explained by the burning in of narrow spectral lines. This additional loss of gain is caused by occasional exposure to the 90″ wide movie slit. A correction can be applied to the data by combining the He I 58.4 nm peak intensity history with the average movie slit exposure pattern.

- The widths of strong lines show a narrowing over time after the burn-in correction has been applied. The narrowing shows a strong correlation with the amount of burn-in. This can be explained by an undercorrection in the wings of the line. The greatest amount of narrowing since the beginning of the mission is 8%, in the 58.4 nm line.
- Some lines, from particularly hot ions, show a small amount of increased burn-in in the vertical center of the slit, evidently due to the practice of centering active regions within the field-of-view.

It should be pointed out that the VDS detector was only lightly scrubbed before delivery, and that a considerable length of time elapsed between delivery of the intensifier section and launch. A more stringent scrubbing policy would have slowed the subsequent burn-in of the average illumination pattern. However, it was decided not to heavily scrub the detector, as the effects of this scrubbing were expected to be lost during the long period of integration, test, and storage before launch.

Because of the high count rates encountered in solar research, future flights of intensified CCD detectors will need to take the differential scrubbing effects discussed here into account. Designs which minimize the effect of the differential scrubbing are to be encouraged. For example, fiber optic coupling of the intensifier to the CCD[6] would reduce the amount of amplification needed in the MCP. Consideration should also be given to providing onboard an even illumination source for both scrubbing and flat-fielding, either in the form of electrons or photons.

11. ACKNOWLEDGMENTS

The author would like to thank O. H. W. Siegmund for his help in confirming the configuration of the MCP. This work was supported by NASA grant NAS5-32350.

REFERENCES

1. R. A. Harrison *et al.*, "The Coronal Diagnostic Spectrometer for the Solar and Heliospheric Observatory," *Solar Phys.* **162**, pp. 233–290, 1995.
2. W. T. Thompson, A. I. Poland, O. H. W. Siegmund, M. Swartz, D. B. Leviton, and L. J. Payne, "Measurements of an intensified CCD detector for the Solar and Heliospheric Observatory," in *EUV, X-ray and Gamma-Ray Instrumentation for Astronomy III*, *Proc. SPIE* **1743**, pp. 464–474, 1992.
3. O. H. W. Siegmund, K. Coburn, and R. F. Malina, "Investigations of large format microchannel plate Z configurations," *IEEE Transactions on Nuclear Science* **32**, p. 443, 1985.
4. N. W. Griffiths, S. Airieau, and O. H. W. Siegmund, "In-flight performance of the SUMER microchannel plate detectors," in *EUV, X-ray and Gamma-Ray Instrumentation for Astronomy IX*, *Proc. SPIE* **3445**, pp. 566–577, 1998.
5. V. A. Drake, F. G. Eparvier, W. E. McClintock, T. N. Woods, G. Ucker, and C. Hill, "Microchannel plate performance and life-test results for the TIMED solar EUV experiment," in *EUV, X-ray and Gamma-Ray Instrumentation for Astronomy IX*, *Proc. SPIE* **3445**, pp. 603–614, 1998.
6. M. Swartz, C. E. Condor, J. M. Davila, J. P. Haas, S. D. Jordan, D. L. Linard, J. J. Miko, I. C. Nash, J. Novello, L. J. Payne, T. B. Plummer, R. J. Thomas, L. A. White, J. W. Brosius, and W. T. Thompson, "The SERTS-97 rocket experiment to study activity on the Sun: Flight 36.167-GS on 1997 November 18," Tech. Rep. TP-1999-208640, NASA Goddard Space Flight Center, Greenbelt, MD 20771, February 1999.